JOURNAL OF THE ROYAL SOCIETY Interface

rsif.royalsocietypublishing.org

Research

Cite this article: Dobrzyński M, Nguyen LK, Birtwistle MR, von Kriegsheim A, Blanco Fernández A, Cheong A, Kolch W, Kholodenko BN. 2014 Nonlinear signalling networks and cell-to-cell variability transform external signals into broadly distributed or bimodal responses. *J. R. Soc. Interface* **11**: 20140383. http://dx.doi.org/10.1098/rsif.2014.0383

Received: 11 April 2014
Accepted: 5 June 2014

Subject Areas:
systems biology, computational biology, biophysics

Keywords:
bimodality, cell heterogeneity, dose–response, signalling networks

Authors for correspondence:
Maciej Dobrzyński
e-mail: maciej.dobrzynski@ucd.ie
Boris N. Kholodenko
e-mail: boris.kholodenko@ucd.ie

Electronic supplementary material is available at http://dx.doi.org/10.1098/rsif.2014.0383 or via http://rsif.royalsocietypublishing.org.

Royal Society Publishing

Nonlinear signalling networks and cell-to-cell variability transform external signals into broadly distributed or bimodal responses

Maciej Dobrzyński[1], Lan K. Nguyen[1], Marc R. Birtwistle[1,6], Alexander von Kriegsheim[1], Alfonso Blanco Fernández[2], Alex Cheong[1,5], Walter Kolch[1,3,4] and Boris N. Kholodenko[1,3,4]

[1]Systems Biology Ireland, [2]Flow Cytometry Core Technologies, Conway Institute of Biomolecular and Biomedical Research, [3]Conway Institute of Biomolecular and Biomedical Research, and
[4]School of Medicine and Medical Science, University College Dublin, Belfield, Dublin 4, Ireland
[5]School of Life and Health Sciences, Aston University, Birmingham B4 7ET, UK
[6]Icahn School of Medicine at Mount Sinai, One Gustave L. Levy Place, Box 1603, New York, NY 10029, USA

MD, 0000-0002-0208-7758; AC, 0000-0003-2482-9078

We show theoretically and experimentally a mechanism behind the emergence of wide or bimodal protein distributions in biochemical networks with nonlinear input–output characteristics (the dose–response curve) and variability in protein abundance. Large cell-to-cell variation in the nonlinear dose–response characteristics can be beneficial to facilitate two distinct groups of response levels as opposed to a graded response. Under the circumstances that we quantify mathematically, the two distinct responses can coexist within a cellular population, leading to the emergence of a bimodal protein distribution. Using flow cytometry, we demonstrate the appearance of wide distributions in the hypoxia-inducible factor-mediated response network in HCT116 cells. With help of our theoretical framework, we perform a novel calculation of the magnitude of cell-to-cell heterogeneity in the dose–response obtained experimentally.

1. Introduction

Thermal fluctuations inherently affect all biochemical reactions, and the variability in molecular copy numbers owing to stochastic effects decreases, as the mean number of molecules in the system rises. Gene expression is inevitably stochastic, as usually there are not more than two gene copies in a cell. It is because of this biochemical noise that cells within an isogenic population, be it a bacterial colony or mammalian cells, at any given point in time exhibit a distribution of measurable properties rather than exhibit a precise value. Cells in genetically identical populations vary in, for example, size, the concentrations of proteins and mRNA, and the stage of progression along the cell cycle.

Quantification of biochemical noise requires single-cell techniques [1–5] capable of reconstructing the whole histogram (a distribution) of molecule counts over the entire cellular population. A bimodal (a double-peaked) distribution is particularly interesting from the physiological point of view, as it indicates existence of two subpopulations with (possibly) distinct phenotypic features. For instance, a bimodal distribution of antibiotic-resistance protein, ZeoR, was suggested to increase viability of the yeast population treated with large doses of Zeocin [6]. In another study, heterogeneous response to treatment with a chemotherapeutic drug, camptothecin, resulted in a bimodal distribution of 24 protein accumulation slopes. Additionally, for the RNA helicase DDX5 and the replication factor RFC1, peaks of their bimodal distributions correlated with different cell fates: fast protein accumulation was found in cells that

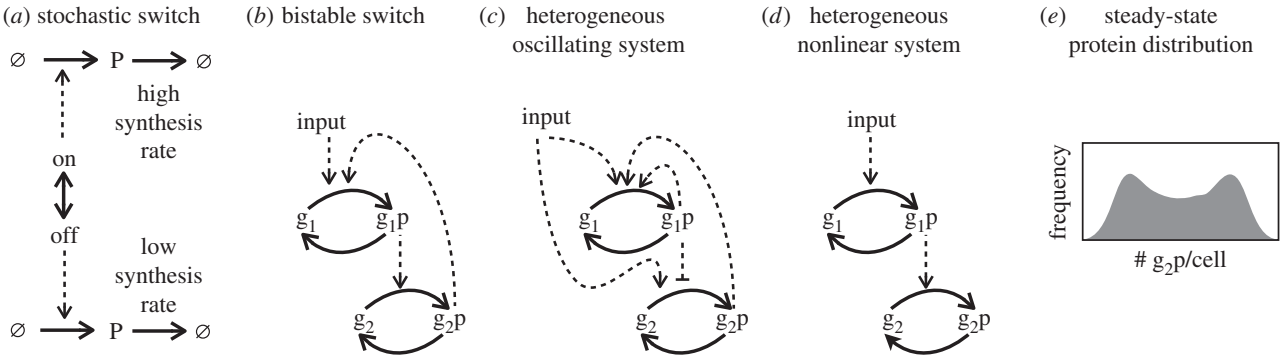

Figure 1. Generic mechanisms that can give rise to bimodal steady-state protein distributions on the cell population level. (*a*) Spontaneous switching between active and inactive state of the promotor [9]. (*b*) Network bistability is brought about by positive feedback [10–12]. (*c*) Oscillating protein abundances in the presence of cell-to-cell variability in oscillations period and/or phase [13]. (*d*) A network with nonlinear input–output characteristic subjected to intrinsic and/or extrinsic noise [14–16]. (*e*) An example of a histogram of steady-state protein concentrations from individual cells as obtained with flow cytometry. Bimodality can arise in the population of cells driven by any of the mechanisms shown in (*a–d*).

survived the treatment, whereas slow accumulation existed in cells undergoing changes associated with cell death [7,8].

In biological systems, bimodal distributions of protein concentrations at the population level can be generated by several mechanisms (figure 1). A genetic switch is the simplest mechanism. For a large difference between the rate of gene on/off switching and the turnover of the gene product, for example, mRNA [9,17], two distinct peaks of product abundance arise (figure 1*a*). Such infrequent gene expression bursts leading to bimodality have been observed in *Escherichia coli* [18], yeast [19] and mammalian cells [2].

In the context of signalling networks, bistability is a well-known mechanism that can generate bimodal responses. It usually requires positive feedback that may be hidden or explicit (figure 1*b*) [10–12,20] or double negative feedback, as in synthetic toggle switch [21]. While stochastic switching requires non-deterministic analysis in order to show the existence of two states, bistable systems can be analysed deterministically with classical ODEs. Importantly, bistability in the deterministic setting does not necessarily lead to bimodal distributions. Dynamic switching between two stable states has to be promoted by fluctuating biochemical reactions or by external noise [22], or by cell-to-cell variability in the thresholds for switching between two steady states [14,23].

A much less appreciated mechanism capable of generating population-level bimodality relies on independently oscillating cells [13]. Cell-to-cell variability in protein abundances affects the period and/or phase of cells' oscillations which in turn generates a bimodal protein distribution (figure 1*c*). The existence of this distribution depends on the extent to which phases of oscillations vary between the cells (*phase mixing*) as well as the functional form of oscillations, for example, pure triangle wave will fail to generate bimodality. Notably, if cells oscillate with a slightly variable period, then the emergence of a bimodal distribution is inevitable with time.

The nature of the mechanism leading to bimodality that we discuss here differs from that of stochastic switching, bistability or superposition of oscillations. Here, two distinctive peaks in steady-state distributions of protein concentrations that arise on the population level stem from the interplay of two factors: (i) nonlinear input–output characteristic (the response) of the biochemical network at the single-cell level [24,25], and (ii) cell-to-cell variability in the abundance of network components which translates to different input–output characteristics of that network across the population (figure 1*d*).

In the following sections, we investigate analytically and numerically how bimodal steady-state protein distributions can emerge in nonlinear biochemical networks. We explore the effect of heterogeneity in the input signals (extrinsic noise) and/or variability in the input–output relationship owing to stochastically expressed network components (intrinsic noise) on the population-level distributions of protein concentrations. We apply our theoretical framework to infer variability in dose–responses across the cellular population from flow-cytometric measurements in the hypoxia response signalling system. We use a mathematical model of this system to demonstrate possible contributions to variability of the dose–response.

2. Results

2.1. Variability of response thresholds

The dose–response characteristics is a relationship between the magnitude of the input stimulus (e.g. growth factor concentration) and the output target, which can be the concentration of an active kinase (such as doubly phosphorylated MAPK) or a transcription factor. It is a function that depends both on the concentration of network components and kinetic parameters of biochemical reactions that involve these components. This input–output relationship, $R(x)$, is commonly approximated by a Hill curve parametrized by four coefficients (β, x_{50}, $R_{\max}$ and H):

$$y = R(x, x_{50}, \beta, R_{\max}, H) = \beta + R_{\max}\frac{x^{H}}{x_{50}^{H} + x^{H}}, \qquad (2.1)$$

where x is the input signal (e.g. concentration of a drug or a toxin), β is basal response level, $R_{\max}$ is the maximum output level and H is the Hill coefficient that determines the steepness of the response. The parameter x_{50} is the response threshold, also known as the half maximal effective concentration (EC_{50}). It is the concentration of the stimulus (the input x) for which the response assumes half of the maximum output (minus basal level).

We assume that cells within a population experience the same level of stimulation x. This condition holds, during

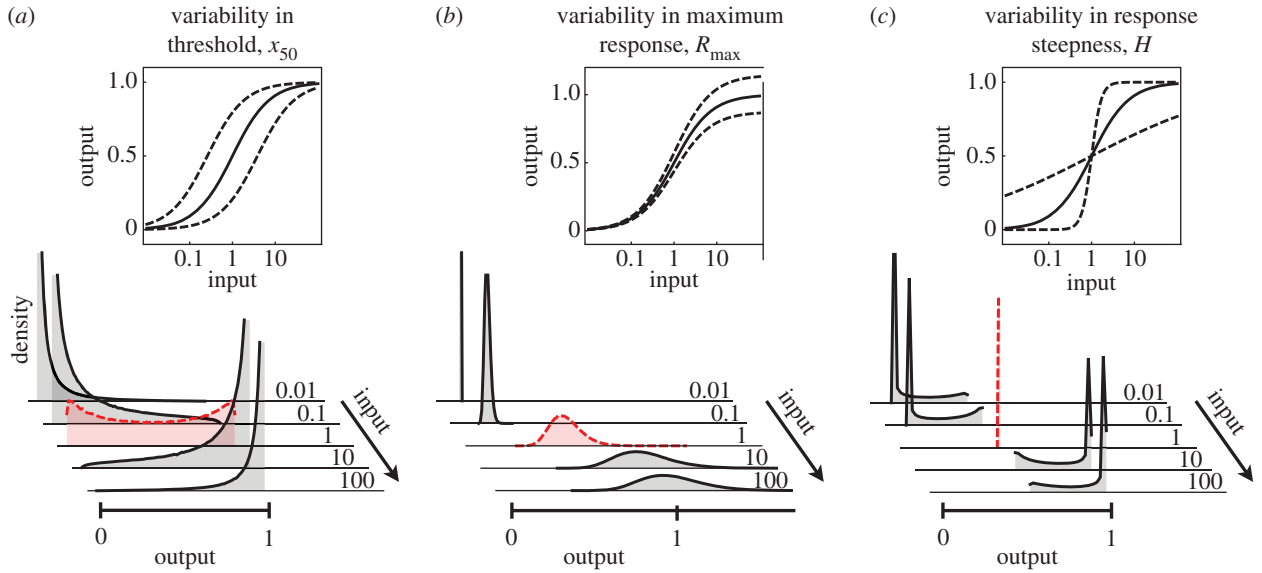

Figure 2. Protein distributions arising from variability of different parameters in the Hill-type response of a nonlinear network. Solid lines in upper panels—response function from equation (2.1) with $\beta = 0$, $x_{50} = 1$, $R_{max} = 1$, $H = 1$. Dashed lines indicate the middle 50% of dose–responses when the indicated parameter is randomly sampled from a lognormal distribution with (*a*) median, $m_{x_{50}} = 1$ and shape parameter $\sigma_{x_{50}} = 2$, (*b*) $m_{R_{max}} = 1$, $\sigma_{R_{max}} = 0.2$, (*c*) $m_H = 1$, $\sigma_H = 2$. Shown in bottom panels are output distributions for a range of inputs. Red dashed—distribution for the input stimulus $x = 1$, which is the midpoint of the averaged dose–response. (Online version in colour.)

our experiments, when cells are grown in a monolayer in a tissue culture and are subjected to equal levels of treatment (input). What sets cells apart is the threshold x_{50} of the response function R. Such variability may stem from differences in the molecule numbers of the same network components and fluctuations in their activation levels. In mathematical terms, we describe this variability by the probability density function (pdf) of thresholds, $f_{x_{50}}(x)$. The resulting distribution of output y for a given input value x in the presence of variable thresholds x_{50} of the response function R is given by a general expression (electronic supplementary material, equations (S1)–(S3)),

$$f_{out}(y) = -f_{x_{50}}(r_{x_{50}}(y)) \cdot \frac{d}{dy} r_{x_{50}}(y), \tag{2.2}$$

where $r_{x_{50}}(y)$ is the inverse of the response function calculated with respect to threshold x_{50}. Note the 'minus' sign, which reflects the fact that the response function is monotonically decreasing with x_{50}.

2.2. Existence of bimodality

Intuitive conditions for the existence of bimodality can be obtained for a model system with Hill-type response function and lognormally distributed threshold x_{50} across the population. It can be demonstrated numerically that such a parameter distribution is indeed a reasonable approximation for signalling cascades with concentrations of network components lognormally distributed across the cellular population (electronic supplementary material, figure S4). The assumption behind the distribution of protein concentrations is justified in the light of experimental evidence. Measurements have shown that protein distributions are lognormal around the mean with additional power-law tails that may arise from feedbacks in biochemical networks [26–28].

The first condition, necessary but not sufficient, relates the steepness H of the dose–response with the shape parameter $\sigma_{x_{50}}$ of the lognormal distribution of x_{50} (electronic supplementary material, equation (S5)),

$$H \cdot \sigma_{x_{50}} > \sqrt{2}, \tag{2.3}$$

where $\sigma_{x_{50}}$ is related to the squared coefficient of variation of x_{50} distribution, $CV^2_{x_{50}}$, through: $\sigma_{x_{50}} = \sqrt{\log(CV^2_{x_{50}} + 1)}$. Thus, steep (large H) steady-state response function R prompts a bimodal distribution even for very narrowly distributed thresholds (small $\sigma_{x_{50}}$). And vice versa, bimodality may result from very heterogeneous but graded (small H) response function R.

Once H and $\sigma_{x_{50}}$ satisfy equation (2.3), a bimodal output distribution may arise but only when the input stimulus, x, is within the steep region of the mean response curve. Parameters H and $\sigma_{x_{50}}$ determine the width of that range. Bimodality will therefore ensue as long as the ratio of the input to the median of the threshold distribution, $m_{x_{50}}$, satisfies

$$\alpha^-(H, \sigma_{x_{50}}) < log\frac{x}{m_{x_{50}}} < \alpha^+(H, \sigma_{x_{50}}), \tag{2.4}$$

where $\alpha^{\mp}(H, \sigma_{x_{50}})$ depends only on H and $\sigma_{x_{50}}$ (electronic supplementary material, equation (S15)). The range of admissible $x/m_{x_{50}}$ ratios widens for a steep dose–response and/or large threshold variability (electronic supplementary material, figure S2).

The Hill function is linearly dependent only on β and R_{max}, hence variability in neither of these parameters alone can generate a bimodal output distribution (figure 2*b*). Variability in H can also introduce bimodality, however, for inputs around the midpoint of the dose–response the distribution reverts to unimodal (figure 2*c*). Because protein distributions for a range of input stimuli that we observe experimentally correspond to those shown in figure 2*a*, we assume that variability in response threshold x_{50} contributes the most to the population-level protein variability.

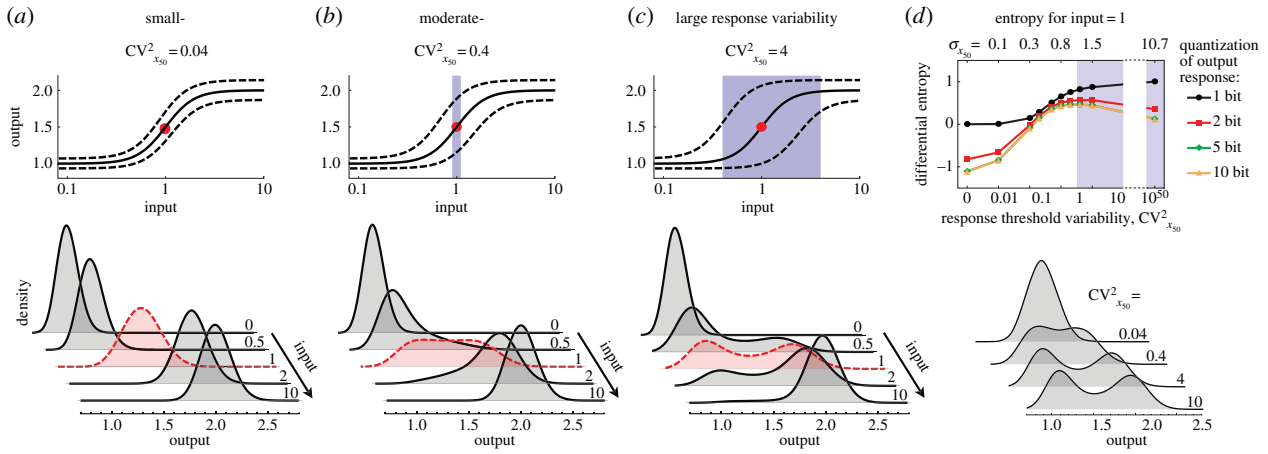

Figure 3. The effect of variability in the response threshold on protein activity distributions. The response steepness $H = 3$. The response threshold is drawn from a lognormal distribution with median $m_{x_{50}} = 1$ and shape parameter $\sigma_{x_{50}} = 0.20$, 0.58 and 1.27 for (a–c) respectively. In addition, lognormally distributed is the baseline, ($m_\beta = 1$, $\sigma_\beta = 0.1$), and maximum response, ($m_{R_{max}} = 1$, $\sigma_{R_{max}} = 0.1$). Dashed lines on both sides of the dose–response (solid line) indicate the middle 50% of responses resulting from variability in β, R_{max} and x_{50}. Red dot is the midpoint (half-maximum) of the dose–response. (d) Differential entropy of output distributions for input level 1 (red dot in (a–c)) as function of threshold variability. Because distributions in a–c are sampled numerically, Shannon entropy is calculated for decreasing histogram bin sizes dy (or increasing quantizations n such that $dy = 1/2^n$) to give the best approximation of the entropy of the continuous density, i.e. the differential entropy [34]. The differential entropy is approximately Shannon entropy of an n-bit quantization of the varying response level, minus n. (a–d) Shaded regions indicate the range of inputs for which the distributions become bimodal and the value of *pdf* at the antimode is lower than 97% of the *pdf*'s value at the minor mode. (Online version in colour.)

Variability in the input stimulus x is mathematically equivalent to variability in x_{50}; therefore, it is equally capable of generating bimodal distributions as has been argued previously in the context of transcriptional regulation [15,29–31]. In those scenarios, variable input signal corresponds to a noisy concentration of a regulatory protein, for example, a transcription factor. By fixing threshold x_{50} in equation (2.1) and by treating x as a variable subjected to fluctuations described by a lognormal distribution, we obtain conceptually similar results as previously. The first condition is the same as previously stated in equation (2.3) with the only difference that σ relates to the variability of the input stimulus rather than to the threshold. The interpretation of the second condition changes accordingly. Function $\alpha^{\mp}(H, \sigma_x)$ bounds the ratio of the input distribution's median m and now fixed threshold level x_{50}.

Equations (2.3) and (2.4) that warrant bimodal system response are derived for a specific case of a lognormal input or response threshold distribution and a Hill-type dose–response. However, the interpretation of the two conditions also holds for other types of distributions and responses, for example, gamma distribution, sigmoidal and logistic response characteristics. Equation (2.3) simply states that in order to facilitate a bimodal distribution both the steepness of the response and variability of thresholds must be coupled; reduction of the former requires an increase in the latter and vice versa. Equation (2.4) prescribes how far the midpoint of the threshold distribution (its 'centre of mass') can be from the midpoint of the response (the steepest point) in order to maintain bimodality. These two conditions hold for other cases as well, although their exact mathematical form is not as simple as for lognormal distribution and Hill-type response. Notably, bimodality may arise only for nonlinear response characteristics. A linear dose–response would result in a trivial result where the output distribution is simply a rescaled distribution of a given parameter in that response function.

Additionally, in order to generate bimodality, the dose–response cannot equal the cumulative distribution (CDF) of the variable parameter or, equivalently, the distribution cannot be a derivative of the response function [32]. If this is the case, then the output distribution becomes uniform on the interval between the lowest and highest response. Consider a cell population with the response function $R(x; x_{50}, H) = x^H/(x_{50}^H + x^H)$ and the threshold distribution across the ensemble $f_{x_{50}}(x_{50}; x, H)$ equal to the derivative of R with respect to x_{50} (with a minus sign). Because $f_{x_{50}}$ depends also on the input stimulus x, the population-level response to any input value is a uniform distribution between 0 and 1. It implies that any signal evokes the exact same population-level response. However, from the biological perspective, the scenario in which the dose–response always remains equal to the CDF of the threshold distribution is intriguing, yet unlikely. It requires x_{50} distribution to change with x, which in turn would affect the dose–response curve. In a more plausible scenario, the system adapts its dose–response to the distribution of inputs that it experiences. It has been shown that a number of neural systems use the strategy of matching the dose–response to CDF of inputs in the environment [32,33] to fully use neuron's limited response range and maximize the information transfer: the most frequently perceived stimuli evoke outputs from the steepest region of the dose–response. Arguably, cellular signalling networks as discussed throughout this paper undergo this type of adaptation.

According to equation (2.4), the range of input/median ratios for which bimodality arises depends on the width of the threshold distribution, $\sigma_{x_{50}} = \sqrt{\log(\mathrm{CV}_{x_{50}}^2 + 1)}$ (electronic supplementary material, figure S2). The larger it is, the stronger the separation of the heterogeneous population into two groups with distinct levels of protein concentrations. Figure 3a–c depicts this intriguing property that runs counter to the conventional assumption that cellular variability destroys robust signalling. Here,

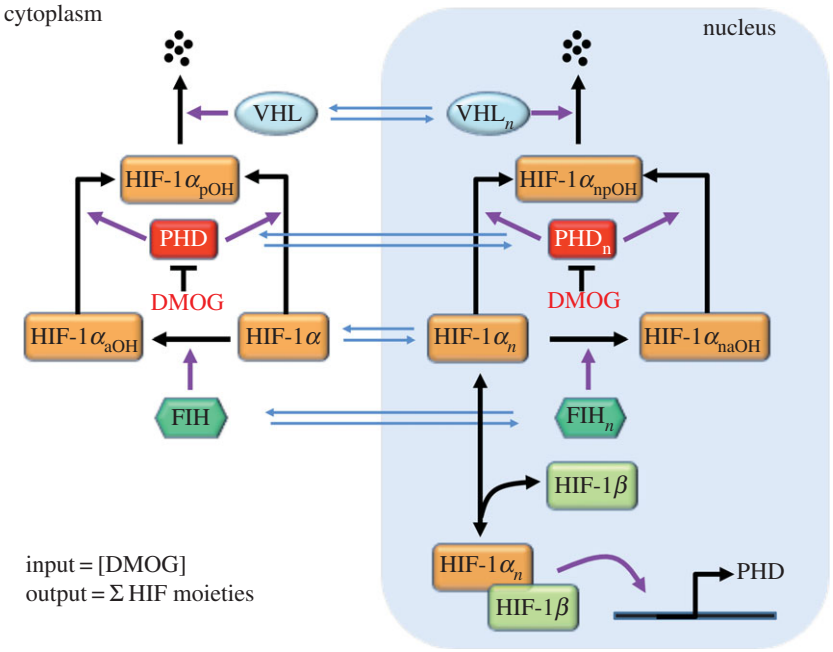

Figure 4. Simplified scheme of the HIF signalling pathway. In both cytoplasm and nucleus (subscript *n*), HIF-1α can be asparaginyl-hydroxylated (aOH) by factor inhibiting HIF (FIH) and/or prolyl-hydroxylated (pOH) by PHD. Prolyl-hydroxylated HIF-1α is targeted for VHL-mediated degradation, whereas asparaginyl-hydroxylated HIF-1α prevents its transcriptional activity. Under DMOG (or hypoxia), PHD is inactivated, leading to HIF-1α protein stabilization and translocation to the nucleus. HIF-1α, PHD, FIH and VHL can shuttle between the nucleus and cytoplasm. Nuclear HIF-1α dimerizes with HIF-1β, creating a transcriptional complex that can bind to the HIF-response elements (HRE) of the target genes, including that of PHD, leading to upregulation of PHD protein and generating a negative feedback loop. (Online version in colour.)

we consider a system with a mildly ultrasensitive, $H = 3$, dose–response. Compare this with $H \approx 5$ reported for the MAPK cascade [24], $H = 5 \ldots 9$ observed for Rap–GTP responding to cannabinoid-1 receptor signal [35], or $H = 1 \ldots 4$ measured for a synthetic system with multiple autoinhibitory modules [36]. For $CV^2_{x_{50}} > 0.4$, protein distributions become significantly wider for input stimuli in the steepest part of the dose–response. For $CV^2_{x_{50}} = 4$, the responses tend to concentrate around basal and saturation values, and two peaks emerge for intermediate stimuli. Such bimodality may facilitate further decision-making, which is not entirely random but is performed based on two well-defined options instead.

Uncertainty of a distribution is often quantified by Shannon entropy [37]. Its low value indicates that a small amount of information is required to describe the varying quantity, for example, protein concentration across the population. Therefore, a peaked unimodal distribution requires a twice shorter description than a bimodal distribution with two narrow peaks. Any wide distribution in between requires more information than either of the two, which is reflected by the high value of entropy. Figure 3*d* quantifies distributions induced by inputs equal to x_{50} of the dose–response (red dots in figure 3*a–c*). The entropy peaks at $CV^2_{x_{50}} \approx 2$ and decreases owing to uncertainty introduced by threshold variability. However, for biologically realistic values of $CV^2_{x_{50}}$ between 0.4 and 4, the distributions change their shape from wide to bimodal, whereas their entropy changes only slightly. This suggests that the quantification of uncertainty using entropy may be misleading as even protein distributions with large entropy may reveal a physiologically relevant widening of a population into two groups. Even though this division is not complete and a number of responses still appear between the peaks, such distributions have been demonstrated to be physiologically advantageous to the population [6].

2.3. Variability in the hypoxia response network

Here, we study experimentally the cellular hypoxia response network, analyse the emergence of wide protein distributions and estimate the response variability from experimental data. When cellular oxygen demand exceeds supply, the cells enter a phase of hypoxia. As a consequence, stabilization of the hypoxia-inducible factor (HIF) ensues. Stabilized HIF mediates transcription of genes to adapt to the hypoxic insult [38]. Central to the response is the action of prolyl-hydroxylases (PHD), enzymes that hydroxylate HIF at residues Pro-402 and Pro-564 [39] and target it for ubiquitination–degradation via the von Hippel–Landau protein (VHL) [40]. Figure 4 depicts a simplified scheme of the network.

For our experimental set-up, we used a stable HCT116 cell line expressing a fragment of the HIF protein containing residues 403–603, termed the oxygen-dependent degradation (ODD) domain [41] tagged to GFP (cells courtesy of Prof. E. Gottlieb [42]). The ODD–GFP is our readout of the hypoxic response. We activate the system using the hydroxylase inhibitor dimethyloxalylglycine (DMOG), which mimics the condition of low oxygen levels in the HIF system [43]. Cells in tissue culture were grown up to 70% confluency at the end of the treatment, which minimized the effect of cell contact and maintained cells in a monolayer such that all of them were exposed to equal levels of DMOG. Hence, any variability in the response can be attributed to intrinsic variations of network components in individual cells, which facilitates our aim of measuring dose–response variability while assuming a fixed input. The condition, however, may

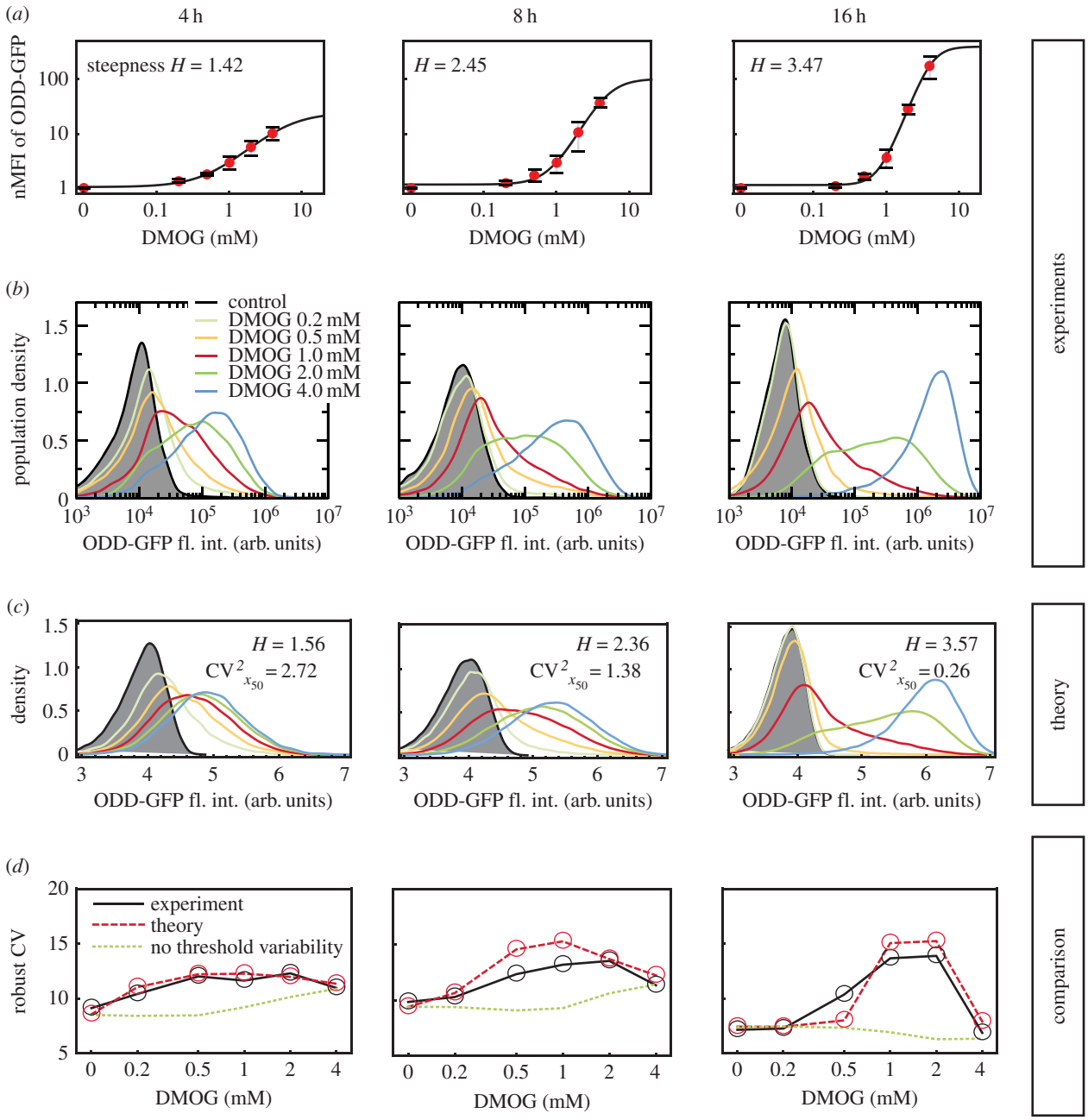

Figure 5. Experimental and theoretical ODD–GFP concentration distributions owing to DMOG treatment in the HIF-response system. (*a*) Dose–response of ODD–GFP to DMOG. Points—flow-cytometric measurement of normalized median fluorescence intensity (nMFI), equation (4.1) in Material and methods, averaged over three or four biological replicates. Error bars indicate 1 s.d. Solid lines—best fits of the Hill equation (2.1). Fitting parameters listed in the electronic supplementary material, table S1. (*b*) Flow-cytometric measurement of ODD–GFP fluorescence intensity (FL1-A) obtained from a single biological repeat at 4, 8 and 16 h post-DMOG. Calculated from 10 000 cells in final gating. (*c*) ODD–GFP distributions computed by Monte Carlo sampling of equation (2.1). Distributions of Hill parameters are fitted to experimental data from row B. Shown are fitted values of H and $\mathrm{CV}^2 = \mathrm{variance}/\mathrm{mean}^2$ of the threshold distribution. See the electronic supplementary material, figure S5 and tables S2–S5. (*d*) Solid line, robust CV (rCV), equation (4.2) in Material and methods, for experimental data from row B; dashed line, rCV for theoretical ODD–GFP concentration distributions from row C; dotted line, rCV with variability in response thresholds, $\sigma_{x_{50}}$, set to zero and the mean set to the mean of the fitted threshold distribution. (Online version in colour.)

not hold in general, especially when cells are embedded in tissue and/or subjected to different microenvironments.

2.4. Hypoxia-inducible factor responses to dimethyloxalylglycine averaged over the cell population

Using flow cytometry, we first identify a sigmoidal dose–response. For each DMOG condition, we calculate the median of the single-cell ODD–GFP fluorescence across a population of a minimum of 10 000 cells. In doing so, we derive the dose–response curve, i.e. the ODD–GFP response to DMOG. We normalize the median to control, unstimulated case. The median response averaged over a minimum of three biological repeats at 4, 8 and 16 h following DMOG addition is shown in figure 5*a* where we also fit the Hill model from equation (2.1) (electronic supplementary material, table S1). The increase with time of the steepness, H, and the maximum response, $R_{\max}$, is consistent with earlier measurements using

Western blots [44], which support the qualitative correspondence between population-averaged flow-cytometric and bulk measurements.

2.5. Hypoxia-inducible factor response distributions across the cell population

Distributions of ODD–GFP fluorescence intensity (figure 5*b*) increase their width for DMOG = 1 and 2 mM. At these DMOG concentrations, the response curve is the steepest; it is the most sensitive region of the cellular response. Widening of the ODD–GFP distribution for DMOG concentrations that induce the steepest region of the dose–response hints at the existence of cell-to-cell variability in response thresholds (cf. figure 2). If there were no threshold variability, then cells treated with DMOG would exhibit a peak of ODD–GFP distribution shifting towards higher values without increase in its width as shown in figure 3*a*. This is not what we observe experimentally. In the presence of threshold variability and steep nonlinear response, the distribution may widen or even become 'split' between the low and high response—the fact quantified by equations (2.3) and (2.4), and illustrated by figure 3*b*,*c*. Consistently with our predictions, the observed widening of the ODD–GFP distribution becomes more pronounced the steeper the dose–response, and the larger, the maximum response level. This is the case at 8 and 16 h post-treatment.

As a next step, we estimate distributions of parameters β, $R_{\max}$ and x_{50} in the Hill model, equation (2.1), from a single experiment. Parameter H is assumed to be constant across the population, and we calculate it by fitting the Hill curve to population-averaged dose–responses (electronic supplementary material, figure S5*a* and table S2). The distribution of basal level β is obtained from the ODD–GFP distribution measured for the unstimulated case, DMOG = 0 mM (electronic supplementary material, figure S5*b* and table S3). Based on our fits of the Hill function to the dose–response, we recognize that even at DMOG = 4 mM the curve does not saturate. However, the ODD–GFP distribution at 8 and 16 h post-DMOG treatment becomes left-skewed, which indicates that the system is not far from saturation. Because higher DMOG levels would be toxic to cells, we decide to use the response at DMOG = 4 mM as a proxy of $R_{\max}$ variability. At that DMOG level, the response is also affected by an independent contribution from variability in the basal level β. We therefore subtract the mean and variance of β from the distribution owing to DMOG = 4 mM and use this new distribution as an estimate of $R_{\max}$ variability (electronic supplementary material, figure S5*c* and table S4).

Finally, we estimate variability in threshold x_{50}. At a given time point, for every DMOG concentration, we record the value of ODD–GFP distribution at a half-distance between the mode (the peak) of the basal (DMOG = 0 mM and the maximum (DMOG = 4 mM) distribution. Such a curve, which is a function of DMOG level, is largely independent of β, $R_{\max}$ and H, and is determined only by parameters of x_{50} distribution. The independence is exact when x_{50} is distributed lognormally (electronic supplementary material, equation (S17)). After normalization to 1, the function has the interpretation of the probability density, which can be used to determine parameters of the x_{50} distribution (electronic supplementary material, figures S3 and S5*d* and table S5).

For spread of parameters β and $R_{\max}$ across the cell population, we fit gamma, lognormal and Weibull distributions. Based on Akaike information criterion [45], we conclude that Weibull distribution is the best approximation of experimentally measured variability in both parameters (electronic supplementary material, figure S5*b*,*c* and tables S3 and S4). By applying these distributions to equation (2.1), we numerically calculate ODD–GFP distributions shown in figure 5*c*. Figure 5*d* quantifies the agreement between experimental and predicted ODD–GFP distributions with a dimensionless robust coefficient of variation, rCV, expressed by equation (4.2) in Material and methods.

According to our model, wide distributions that we observe experimentally can arise only in the presence of variability in the response threshold, x_{50} (figure 2). We find that the dimensionless squared coefficient of variation (CV^2 = variance over squared mean) of fitted x_{50} distribution decreases from 2.72 at 4 h, through 1.38 at 8 h, down to 0.26 at 16 h post-treatment. The decrease in $CV^2_{x_{50}}$ over time is compensated by increasing H, which promotes widening of the ODD–GFP distribution at DMOG concentrations that induce the steep part of the response. Substituting H and $CV^2_{x_{50}}$ into equation (2.3) reveals that the system remains in the same regime where only mild bimodality may arise (electronic supplementary material, table S6 and figure S6). The distribution is further affected by variability in β and $R_{\max}$, which results in widening instead of the emergence of two clearly separated peaks. The widening is reflected by the increase in rCV (figure 5*d*). In the case of small x_{50} variability, or lack thereof, an increasing stimulus would induce a proportionally shifting peak of ODD–GFP distribution without widening as illustrated in figure 3*a* and quantified by a theoretical dotted line in figure 5*d*.

2.6. Response variability in a mathematical model of the hypoxia-inducible factor system

We used a published mathematical model of the HIF system [44] to search for possible molecular sources causing large dose–response variability. First, we calculate numerically the response of the system at 16 h to various oxygen tension levels, which affects the HIF level in the opposite manner to DMOG treatment. The untreated case corresponds to 21% of oxygen, i.e. normoxia, whereas high DMOG treatment corresponds to the hypoxic condition of a low oxygen level. The Hill function is then fitted to the calculated dose–response. In order to account for cell-to-cell heterogeneity, we repeat this procedure 1000 times with total levels of all protein species drawn from a lognormal distribution with CV^2 = 0.5 and means fixed to the original ODE model (supplementary material of [44]). The chosen CV^2 is at the upper limit of measured protein variability in mammalian cells which typically ranges between 0.1 and 0.5 [7,16,28,46,47].

The mean and variability of the dose–response obtained from a population of deterministic models are shown in figure 6*a*. By fitting the Hill function to each of the responses from the entire population, we obtain distributions of parameters x_{50}, β, $R_{\max}$ and H at 16 h post-treatment (figure 6*c*–*f*). The distribution of H has the smallest CV^2 of all parameters, which justifies our choice of neglecting variability in H when estimating variability of Hill parameters from experimental data in §2.5. The distribution of x_{50} is well approximated by a lognormal distribution, and

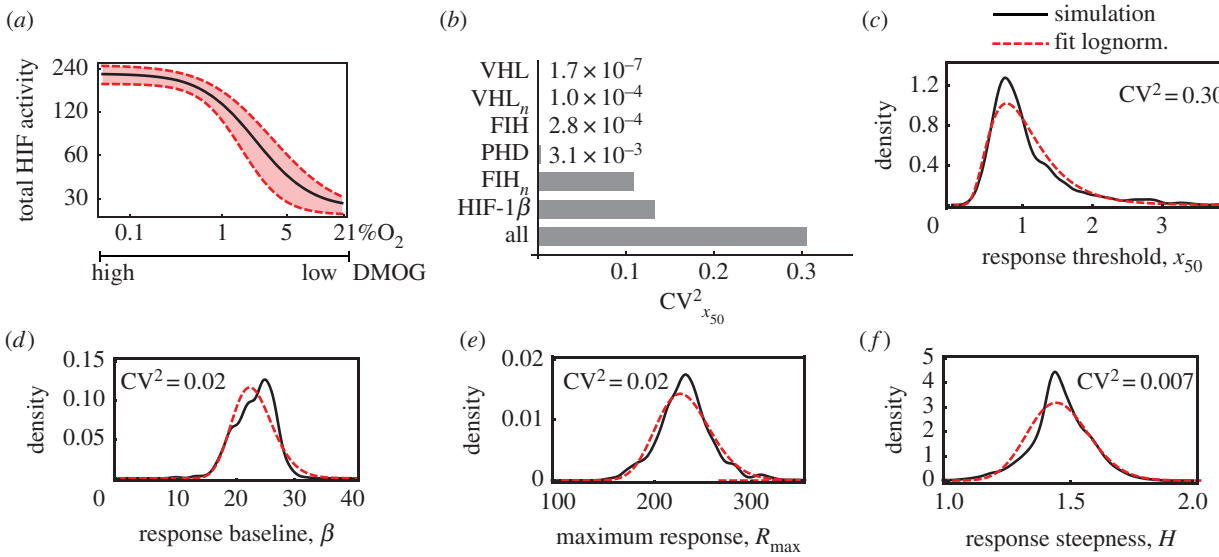

Figure 6. Mathematical model of HIF system demonstrates the effect of variability in protein concentrations on the dose–response. Using a published ODE model [44], we calculate the dose–response at 16 h post-DMOG for an ensemble of systems where the total protein levels are drawn from a lognormal distribution with $CV^2 = 0.5$ and mean: [VHL] = 50, [VHL_n] = 50, [FIH] = 110, [PHD] = 100, [FIH_n] = 40 and [HIF − 1β] = 170 nM. For each of the simulated dose–responses, we fit a Hill function: $\beta + R_{max}\, x_{50}^{H}/(x_{50}^{H} + x^{H})$ and obtain the corresponding parameters. (*a*) Black solid line, the mean response to oxygen level: 21%—normoxia, below 1%—hypoxia (note log scale of *x*-axis). All protein levels are varied. Red dashed line, 1 s.d. (*b*) CV^2 of the response threshold resulting from variability in individual and all protein levels. (*c–f*) Black solid line, simulated probability densities of Hill parameters obtained from an ensemble of fitted Hill functions when all total protein levels are drawn from a lognormal distribution with $CV^2 = 0.5$ (lowest bar in *b*). Red dashed line, best fit of the lognormal distribution. (Online version in colour.)

$CV^2_{x_{50}} = 0.30$ is comparable to 0.26 that we estimated from experimental data in figure 5*c*. Additionally, we perform local sensitivity analysis by randomly sampling total concentrations of individual protein species from a lognormal distribution with the mean as in the ODE model and $CV^2 = 0.5$ while keeping the remaining concentrations fixed. Interestingly, the variability of the response threshold in the HIF model is largely insensitive to variability of the majority of network components (figure 6*b*). The variability in only two protein concentrations, nuclear FIH and HIF-1β, translates to large CV^2 of response thresholds.

3. Discussion

Signalling networks can transform analogue, continuous input signals into distinct low and high response states [48]. The sigmoidal shape of that response is typically a result of layers of phospho- and dephosphorylation cycles (e.g. MAPK cascade [24]) or simply results from nonlinearity of enzymatic reactions as in the case of the HIF network. The steep sigmoidal response minimizes the region where stimuli could result in ambiguous outputs, making such a response characteristic a prevailing biological mechanism on which cellular decision-making can rely. Because of the large number of molecules that eukaryotic signalling networks typically consist of, at the level of a single cell, these systems seem to be protected from undesirable stochastic effects, which can occur at low molecule counts. Still, cells within a population differ in their molecular make-up because of the biochemical noise that affects total protein levels. This randomness affects the shape of the dose–response and causes a similarly random response of a cellular population.

Our theoretical results demonstrate that networks with sigmoidal response characteristics possess yet another fascinating feature, this time at the level of cellular ensemble. In the presence of variability in nonlinear dose–response across the population, two subpopulations can emerge with distinct response levels. The condition being, dose–response needs to be of sufficient steepness. Our analysis provides intuitive mathematical insights into conditions under which such a response in form of a bimodal protein distribution may arise.

Cell-to-cell variability of the dose–response threshold, x_{50}, more commonly known as EC_{50}, is essential for generating wide or bimodal distributions in response to a common input signal. In the absence of such response variability, protein distribution would not widen but shift proportionally to the stimulus (figure 3*a*), which is not what we observed in our experiments. Flow-cytometric analysis of the HIF system demonstrated that the response, measured as ODD–GFP distribution, indeed widens for inputs (DMOG treatment) in the steepest region of the Hill-type dose–response. Our theoretical framework provides a means of estimating EC_{50} variability from flow cytometry data and an explanation of protein distribution widening.

Without EC_{50} variability, the ODD–GFP distribution would not widen as is illustrated by the dotted line in figure 5*d*. Even though the squared coefficient of variation of the response threshold decreased 10 times between 4 and 16 h after DMOG treatment, the steepness *H* of the response increased more than twice over the same period. Together, these two parameters facilitate a necessary but not sufficient condition for bimodality expressed by equation (2.3). After substituting EC_{50} variability and *H*, we find that the system remains approximately in the same regime where only very mild bimodality may arise (electronic supplementary material, table S6 and figure S6). Using our framework, we hypothesize that the response steepness at 16 h post-treatment is sufficient to bring about two distinct peaks in

the response, provided that CV^2 of EC_{50} remained at the level of 2.72 (as estimated at 4 h) throughout the treatment (electronic supplementary material, figure S6).

We have shown that owing to certain features of the nonlinear input–output characteristics commonly observed in cellular signalling networks, random differences between individual cells enable the separation of these cells into subpopulations with distinct responses to the common signal. The significance of our results extends beyond cascaded signalling networks. Any network with nonlinear dose–response characteristics may exhibit bimodal behaviour as shown in our study. In particular, a simple enzymatic reaction or a gene expression network also belong to that class. For all of such nonlinear networks, variability of EC_{50} caused by cell-to-cell differences in protein concentrations is an important factor to consider when designing a perturbation, for example a drug treatment. According to our theory, one of the strategies to avoid the emergence of two subpopulations, low and high responders, is to smooth the dose–response, i.e. decrease the coefficient H. This in turn can be achieved by establishing a negative feedback in the network [14]. Alternatively, the condition expressed by equation (2.3) demonstrates that the output protein distribution can be rid of bimodality by decreasing the variability of dose–response threshold resulting from cell-to-cell variability of network components. With current advancements in synthetic biology and ongoing progress in mathematical modelling of biochemical networks, such interventions in *in vivo* systems will likely become more routine. An intriguing open question is to what extent bimodal population-wide protein distributions brought about by the mechanism discussed here are used to perform physiologically relevant decision-making.

4. Material and methods

4.1. Cell culture

Human colon carcinoma (HCT116) cells stably expressing GFP–ODD were a generous gift from Prof. Gottlieb and were previously used in another study [42]. The cells were subsequently subcloned as single-cell clones by growing cells in DMEM 10% FCS supplemented with 800 μg ml^{-1} G418. The clones were treated with 2 mM DMOG for 16 h. Two clones where eGFP–ODD was induced were selected. Cells were then maintained in a humidified 5% CO_2 incubator at 37°C and cultured in Dulbecco's modified Eagle's medium supplemented with 10% FCS, 1% L-glutamine and 50 μg ml^{-1} G418.

4.2. Flow cytometry

HCT116 cells were treated with cell permeable pan-hydroxylase inhibitor dimethyloxalylglycine (DMOG; Cayman Chemicals, MI, USA) dissolved in DMSO (Sigma, Wicklow, Ireland) and diluted with growth medium to appropriate concentration. The cells were then lifted by trypsinization (0.05% trypsin–EDTA, Gibco) and resuspended in 0.5 ml growth medium with DMOG concentration corresponding to initial stimulation. Experiments were replicated four times for each time point. The samples were analysed with Accuri C6. Post-gating by forward and side scatter was performed to remove events corresponding to dead cells, debris and cell clusters (i.e. doublets). For each sample, 10 000 events (cells) were collected in final gating.

Dose–response from flow cytometry experiments (figure 5) was calculated using normalized median fluorescence intensity (nMFI),

$$\mathrm{nMFI}(\mathrm{stimulus}_i) = \frac{\text{median fluorescence}\,(\mathrm{stimulus}_i)}{\text{median fluorescence}\,(\text{control})}. \quad (4.1)$$

In order to quantify the width of protein distributions obtained from flow cytometry and calculated numerically, we use robust CV (from FlowJo flow cytometry analysis software) defined as follows

$$\mathrm{rCV} = \frac{100}{2} \times \frac{\text{intensity}[84.13\%\text{ile}] - \text{intensity}[15.87\%\text{ile}]}{\text{median intensity}}. \quad (4.2)$$

The rCV is not as sensitive to outliers and gives a better than CV description of the distribution spread on logarithmic scales.

Acknowledgements. We thank Lisa Heiserich for kindly providing us with HCT116 cells and the anonymous reviewers for their insightful comments.

Funding statement. This study is supported by Science Foundation Ireland (under grant no. 06/CE/B1129) and European Union Grant PRIMES (no. FP7-HEALTH-2011-278568).

References

1. Golding I, Cox EC. 2004 RNA dynamics in live *Escherichia coli* cells. *Proc. Natl Acad. Sci. USA* **101**, 11 310–11 315. (doi:10.1073/pnas.0404443101)
2. Raj A, Peskin CS, Tranchina D, Vargas DY, Tyagi S. 2006 Stochastic mRNA synthesis in mammalian cells. *PLoS Biol.* **4**, e309. (doi:10.1371/journal.pbio.0040309)
3. Newman JRS, Ghaemmaghami S, Ihmels J, Breslow DK, Noble M, DeRisi JL, Weissman JS. 2006 Single-cell proteomic analysis of *S. cerevisiae* reveals the architecture of biological noise. *Nature* **441**, 840–846. (doi:10.1038/nature04785)
4. Bengtsson M, Hemberg M, Rorsman P, Ståhlberg A. 2008 Quantification of mRNA in single cells and modelling of RT-qPCR induced noise. *BMC Mol. Biol.* **9**, 63. (doi:10.1186/1471-2199-9-63)
5. Tyson DR, Garbett SP, Frick PL, Quaranta V. 2012 Fractional proliferation: a method to deconvolve cell population dynamics from single-cell data. *Nat. Methods* **9**, 923–928. (doi:10.1038/nmeth.2138)
6. Blake WJ *et al*. 2006 Phenotypic consequences of promoter-mediated transcriptional noise. *Mol. Cell* **24**, 853–865. (doi:10.1016/j.molcel.2006.11.003)
7. Cohen AA *et al*. 2008 Dynamic proteomics of individual cancer cells in response to a drug. *Science* **322**, 1511–1516. (doi:10.1126/science.1160165)
8. Gaudet S, Spencer SL, Chen WW, Sorger PK. 2012 Exploring the contextual sensitivity of factors that determine cell-to-cell variability in receptor-mediated apoptosis. *PLoS Comput. Biol.* **8**, e1002482. (doi:10.1371/journal.pcbi.1002482)
9. Shahrezaei V, Swain PS. 2008 Analytical distributions for stochastic gene expression. *Proc. Natl Acad. Sci. USA* **105**, 17 256–17 261. (doi:10.1073/pnas.0803850105)
10. Schwabe A, Dobrzyński M, Rybakova K, Verschure P, Bruggeman FJ. 2011 Origins of stochastic intracellular processes and consequences for cell-to-cell variability and cellular survival strategies. *Methods Enzymol.* **500**, 597–625.
11. Yu J, Xiao J, Ren X, Lao K, Xie XS. 2006 Probing gene expression in live cells, one protein molecule at a time. *Science* **311**, 1600–1603. (doi:10.1126/science.1119623)
12. Blake WJ, Kærn M, Cantor CR, Collins JJ. 2003 Noise in eukaryotic gene expression. *Nature* **422**, 633–637. (doi:10.1038/nature01546)
13. Becskei A, Séraphin B, Serrano L. 2001 Positive feedback in eukaryotic gene networks: cell differentiation by graded to binary response

conversion. *EMBO J.* **20**, 2528–2535. (doi:10.1093/emboj/20.10.2528)

14. Kholodenko BN. 2006 Cell-signalling dynamics in time and space. *Nat. Rev. Mol. Cell Biol.* **7**, 165–176. (doi:10.1038/nrm1838)
15. Tyson JJ, Baumann WT, Chen C, Verdugo A, Tavassoly I, Wang Y, Weiner LM, Clarke R. 2011 Dynamic modelling of oestrogen signalling and cell fate in breast cancer cells. *Nat. Rev. Cancer* **11**, 523–532. (doi:10.1038/nrc3081)
16. Fey D, Croucher DR, Kolch W, Kholodenko BN. 2012 Crosstalk and signaling switches in mitogen-activated protein kinase cascades. *Front. Physiol.* **3**, 355. (doi:10.3389/fphys.2012.00355)
17. Collins JJ, Gardner TS, Cantor CR. 2000 Construction of a genetic toggle switch in *Escherichia coli*. *Nature* **403**, 339–342. (doi:10.1038/35002131)
18. Samoilov M, Plyasunov S, Arkin AP. 2005 Stochastic amplification and signaling in enzymatic futile cycles through noise-induced bistability with oscillations. *Proc. Natl Acad. Sci. USA* **102**, 2310–2315. (doi:10.1073/pnas.0406841102)
19. Vilar JMG. 2010 Noisy-threshold control of cell death. *BMC Syst. Biol.* **4**, 152. (doi:10.1186/1752-0509-4-152)
20. Birtwistle MR, Rauch J, Kiyatkin A, Aksamitiene E, Dobrzyński M, Hoek JB, Kolch W, Ogunnaike BA, Kholodenko BN. 2012 Emergence of bimodal cell population responses from the interplay between analog single-cell signaling and protein expression noise. *BMC Syst. Biol.* **6**, 109. (doi:10.1186/1752-0509-6-109)
21. Dobrzyński M, Fey D, Nguyen LK, Kholodenko BN. 2012 Bimodal protein distributions in heterogeneous oscillating systems. In *Computational methods in systems biology* (eds D Gilbert, M Heiner), Lecture Notes in Computer Science, pp. 17–28. Berlin, Germany: Springer.
22. Huang CY, Ferrell JE. 1996 Ultrasensitivity in the mitogen-activated protein kinase cascade. *Proc. Natl Acad. Sci. USA* **93**, 10 078–10 083. (doi:10.1073/pnas.93.19.10078)
23. Chen J-Y, Lin J-R, Cimprich KA, Meyer T. 2012 A two-dimensional ERK-AKT signaling code for an NGF-triggered cell-fate decision. *Mol. Cell* **45**, 196–209. (doi:10.1016/j.molcel.2011.11.023)
24. Krishna S, Banerjee B, Ramakrishnan TV, Shivashankar GV. 2005 Stochastic simulations of the origins and implications of long-tailed distributions in gene expression. *Proc. Natl Acad. Sci. USA* **102**, 4771–4776. (doi:10.1073/pnas.0406415102)
25. Lu C, King RD. 2009 An investigation into the population abundance distribution of mRNAs, proteins, and metabolites in biological systems. *Bioinformatics* **25**, 2020–2027. (doi:10.1093/bioinformatics/btp360)
26. Birtwistle MR, von Kriegsheim A, Dobrzyński M, Kholodenko BN, Kolch W. 2012 Mammalian protein expression noise: scaling principles and the implications for knockdown experiments. *Mol. Biosyst.* **8**, 3068–3076. (doi:10.1039/c2mb25168j)
27. Kærn M, Elston TC, Blake WJ, Collins JJ. 2005 Stochasticity in gene expression: from theories to phenotypes. *Nat. Rev. Genet.* **6**, 451–464. (doi:10.1038/nrg1615)
28. Tkacik G, Callan CG, Bialek W. 2008 Information flow and optimization in transcriptional regulation. *Proc. Natl Acad. Sci. USA* **105**, 12 265–12 270. (doi:10.1073/pnas.0806077105)
29. Walczak AM, Mugler A, Wiggins CH. 2009 A stochastic spectral analysis of transcriptional regulatory cascades. *Proc. Natl Acad. Sci. USA* **106**, 6529–6534. (doi:10.1073/pnas.0811999106)
30. Ochab-Marcinek A, Tabaka M. 2010 Bimodal gene expression in noncooperative regulatory systems. *Proc. Natl Acad. Sci. USA* **107**, 22 096–22 101. (doi:10.1073/pnas.1008965107)
31. Bartlett MS. 2007 Information maximization in face processing. *Neurocomputing* **70**, 2204–2217. (doi:10.1016/j.neucom.2006.02.025)
32. Laughlin S. 1981 A simple coding procedure enhances a neuron's information capacity. *Z. Naturforsch., C, Biosci.* **36**, 910–912.
33. Lipshtat A, Jayaraman G, He JC, Iyengar R. 2010 Design of versatile biochemical switches that respond to amplitude, duration, and spatial cues. *Proc. Natl Acad. Sci. USA* **107**, 1247–1252. (doi:10.1073/pnas.0908647107)
34. Dueber JE, Mirsky EA, Lim WA. 2007 Engineering synthetic signaling proteins with ultra-sensitive input/output control. *Nat. Biotechnol.* **25**, 660–662. (doi:10.1038/nbt1308)
35. Cover TM, Thomas JA. 1991 Entropy, relative entropy and mutual information. In *Elements of information theory*, pp. 12–49. New York, NY: John Wiley & Sons.
36. Semenza GL. 2012 Hypoxia-inducible factors in physiology and medicine. *Cell* **148**, 399–408. (doi:10.1016/j.cell.2012.01.021)
37. Schofield CJ, Ratcliffe PJ. 2004 Oxygen sensing by HIF hydroxylases. *Nat. Rev. Mol. Cell Biol.* **5**, 343–354. (doi:10.1038/nrm1366)
38. Bruick RK, McKnight SL. 2001 A conserved family of prolyl-4-hydroxylases that modify HIF. *Science* **294**, 1337–1340. (doi:10.1126/science.1066373)
39. Masson N, Willam C, Maxwell PH, Pugh CW, Ratcliffe PJ. 2001 Independent function of two destruction domains in hypoxia-inducible factor-alpha chains activated by prolyl hydroxylation. *EMBO J.* **20**, 5197–5206. (doi:10.1093/emboj/20.18.5197)
40. Tennant DA *et al*. 2009 Reactivating HIF prolyl hydroxylases under hypoxia results in metabolic catastrophe and cell death. *Oncogene* **28**, 4009–4021. (doi:10.1038/onc.2009.250)
41. Epstein AC *et al*. 2001 *C. elegans* EGL-9 and mammalian homologs define a family of dioxygenases that regulate HIF by prolyl hydroxylation. *Cell* **107**, 43–54. (doi:10.1016/S0092-8674(01)00507-4)
42. Nguyen LK *et al*. 2013 A dynamic model of the hypoxia-inducible factor 1α (HIF-1α) network. *J. Cell Sci.* **126**, 1454–1463. (doi:10.1242/jcs.119974)
43. Akaike H. 1974 A new look at the statistical model identification. *IEEE Trans. Autom. Control* **19**, 716–723. (doi:10.1109/TAC.1974.1100705)
44. Feinerman O, Veiga J, Dorfman JR, Germain RN, Altan-Bonnet G. 2008 Variability and robustness in T cell activation from regulated heterogeneity in protein levels. *Science* **321**, 1081–1084. (doi:10.1126/science.1158013)
45. Niepel M, Spencer SL, Sorger PK. 2009 Non-genetic cell-to-cell variability and the consequences for pharmacology. *Curr. Opin. Chem. Biol.* **13**, 556–561. (doi:10.1016/j.cbpa.2009.09.015)
46. Spencer SL, Gaudet S, Albeck JG, Burke JM, Sorger PK. 2009 Non-genetic origins of cell-to-cell variability in TRAIL-induced apoptosis. *Nature* **459**, 428–432. (doi:10.1038/nature08012)
47. Kholodenko BN, Hancock JF, Kolch W. 2010 Signalling ballet in space and time. *Nat. Rev. Mol. Cell Biol.* **11**, 414–426. (doi:10.1038/nrm2901)
48. Cover TM, Thomas JA. 1991 Differential entropy. In *Elements of information theory*, pp. 224–238. New York, NY: John Wiley & Sons.